Meas. Sci. Technol. 6 (1995) 995–1008. Printed in the UK

A broad-band and high-sensitivity dielectric spectroscopy measurement system for quality determination of low-permittivity fluids

K Folgerø†‡, T Friisø†‡, J Hilland§ and T Tjomsland§

† Stord/Haugesund College, Skåregaten 103, N-5500 Haugesund, Norway
‡ Department of Physics, University of Bergen, Allegaten 55, N-5007 Bergen, Norway
§ Christian Michelsen Research AS, Fantoftvegen 38, N-5036 Fantoft, Norway

Received 30 November 1994, in final form 7 February 1995, accepted for publication 15 February 1995

Abstract. Traditional quality measurement systems in the petroleum-related industry are complex in structure and difficult to maintain. A measurement system for high-sensitivity and accurate permittivity measurements has been built in order to investigate dielectric spectroscopy as a basis for an easier-to-maintain system, which can replace some of the traditional instrumentation systems. The permittivity measurement system has been designed and tested for low-permittivity and low-loss fluids in the frequency range from 1 kHz to 5 GHz. In the lower part of the frequency range impedance measurements are used, and in the higher range reflection coefficient measurements are employed. The characteristics of the measurement cells are optimized to give high sensitivity. High-accuracy permittivity measurements are obtained by calibration with several known fluids. Temperature control and careful experimental routines ensure good repeatability. Estimated overall uncertainty and presented measurement results on low-permittivity and low-loss oils and reference fluids confirm the performance of the system.

1. Introduction

In the petroleum-related industry there is an increasing demand for reliable on-line measurement systems for determination of product quality. Traditionally, measurement systems based upon optical systems have been employed [1, 2]. Infrared and ultraviolet absorption and deflection techniques are well known methods for quality determination [3, 4]. There are, however, large disadvantages involved in the use of on-line optical instrumentation in process streams and especially for opaque fluids. From problems involving maintenance, sampling and sample pre-treatment, not to mention scaling and fouling of the sensors, arises the need for new and more robust instrumentation.

The dielectric properties of petrochemical products can be used to characterize the quality. Important molecular and bulk information can be extracted from the measured permittivity spectra [5]. Dielectric measurement methods may be more robust than optical methods and the technique is not dependent upon the opaqueness of the process fluids. Dielectric spectroscopy is therefore considered as a relevant method for quality determination.

Figure 1 shows a sketch of a laboratory system. The measurement system consists of two measurement cells, an impedance analyser and a network analyser. In the lowest frequency range a linear relationship is used to calculate the permittivity from the measured data. This is found by linear regression of measurements on reference fluids. In the higher frequency ranges a bilinear calibration procedure is used [6, 7]. These models will be described in the following sections.

The curve-fitting is based on the Cole–Cole model [8]:

$$\varepsilon^*(\omega) = \varepsilon' - \mathrm{j}\varepsilon'' = \varepsilon_\infty + \frac{\varepsilon_s - \varepsilon_\infty}{1 + (\mathrm{j}\omega\tau)^{1-\alpha}} - \frac{\mathrm{j}\sigma}{\omega\varepsilon_0} \qquad (1)$$

where $\varepsilon^*(\omega)$ is the relative complex permittivity as a function of frequency, ε' is the real part of the relative permittivity, ε'' is the imaginary part of the relative permittivity containing both conductivity and dielectric

0957-0233/95/070995+14$19.50

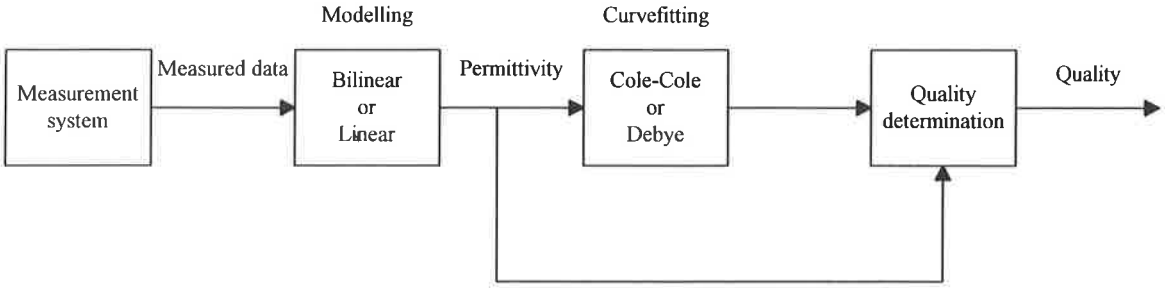

Figure 1. The structure of a laboratory system. The measured data is transferred to permittivity data employing bilinear (high frequencies) or linear (low frequencies) models. Via curve-fitting to Cole–Cole or Debye models, or directly from the permittivity data, the quality determination procedure estimates the quality of the fluid.

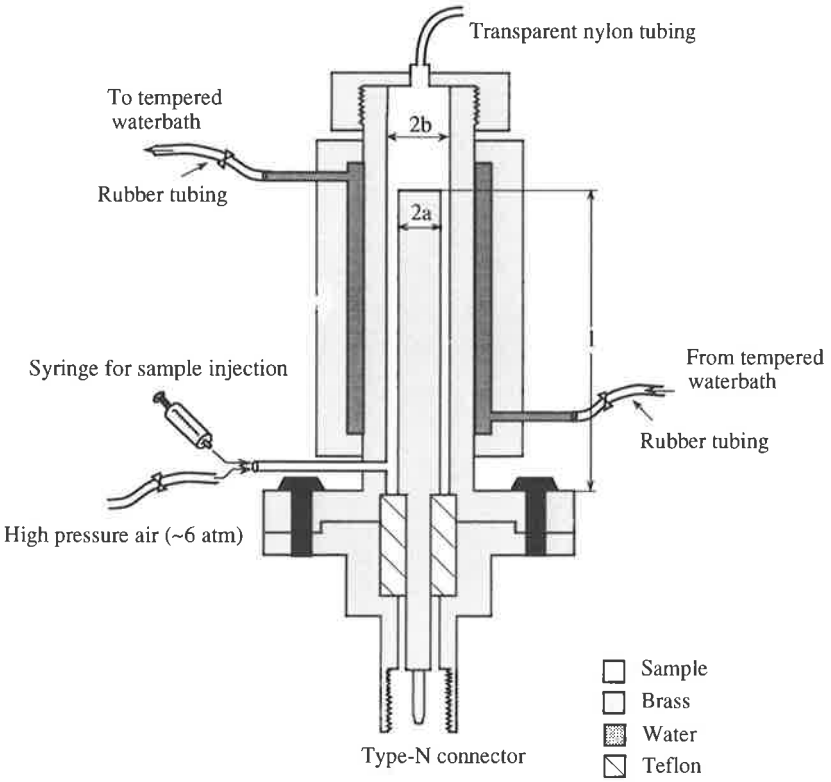

Figure 2. A sketch of the coaxial measurement cell including the temperature control chamber and the sample injection tube. Two versions of this cell are used; one for high frequencies, and one for low and intermediate frequencies.

loss, ε_s is the static relative permittivity, ε_∞ is the optical relative permittivity, ε_0 is the permittivity of vacuum, 8.85×10^{-12} F m^{-1}, ω is the angular frequency (rad s^{-1}), τ is the relaxation time (s), σ is the conductivity of the fluid (S m^{-1}) and α is the distribution factor. When α is zero, the Cole–Cole model is equivalent to the Debye model [9].

The quality determination routine estimates the quality parameters of the fluid from the Cole–Cole parameters or directly from the measured permittivity spectrum. This estimation can be done by chemometric modelling. This paper presents the development and testing of the first part of the laboratory system, namely the high-sensitivity measurement system and the linear and bilinear model which relate the measured data to permittivity.

Oil has low static permittivity and loss, long relaxation times and a broad frequency dispersion region. To determine the important parts of the permittivity spectra, we must be able to measure the permittivity with high sensitivity, precision and repeatability over a broad frequency range. Therefore great care must be taken in designing the measurement system. The design of the measurement cells is especially critical for achieving high sensitivity. Important factors for obtaining high precision and repeatability are good experimental routines, temperature control, high-quality measurement accessories (such as coaxial cables) and adequate models

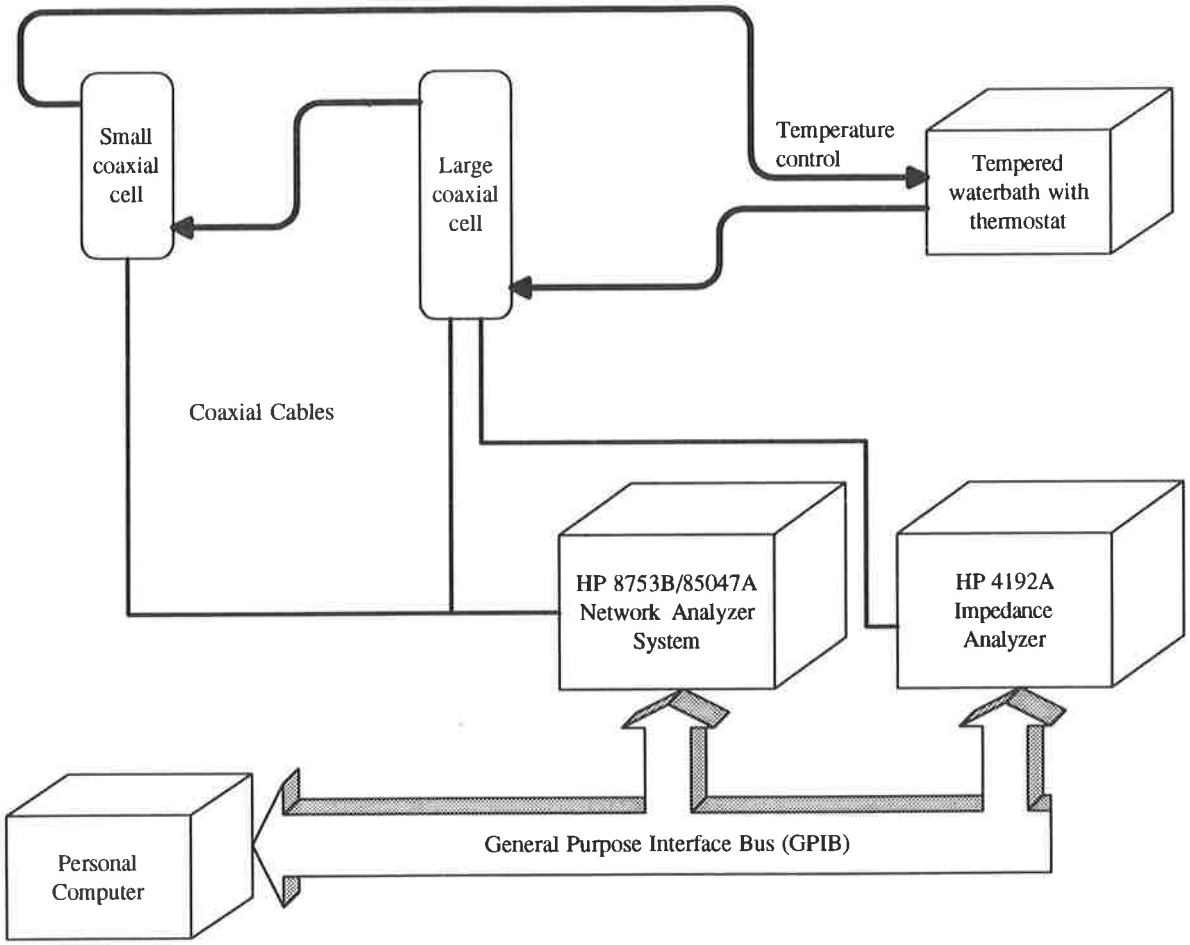

Figure 3. The measurement system consist of the measurement cells, temperature control, impedance analyser, network analyser system and a personal computer. The measurement cells are filled with the fluid under test, the impedance and network analysers determine the impedance and reflection coefficients, respectively. The measured data are transferred to the personal computer for processing and presentation.

for calculating permittivity from measured parameters.

Several cell configurations can be used to measure permittivity in the relevant frequency range [10–14]. It has been shown [7, 15] that open-ended coaxial cells can be designed to meet the sensitivity requirements for this project. Likewise are transmission cells [16–18] and resonance methods [12] usable for higher frequencies. However, open-ended coaxial cells are selected in this work because they are mechanically stable, easy to manufacture and maintain, easy to use and have been well studied and modelled.

2. The measurement system

The system presented in this paper measures the permittivity over a broad frequency range. This requires two different signal analysers and two measurement cells. In addition, the system includes a computer for data acquisition and processing.

A detailed sketch of an open-ended coaxial measurement cell is shown in figure 2. A sample injection tube is incorporated at the bottom of each measurement cell and an overflow pipe is mounted at the top of the cell. This cell is employed both for impedance and for reflection measurements.

The measurement of the complex permittivity is performed in the frequency domain. The frequency range is divided into three sub-ranges, due to different measurement techniques and different measurement cells. In the lowest frequency range (1 kHz to 5 MHz), the impedance of a coaxial cell is measured using an impedance analyser, in the intermediate frequency range (10–100 MHz), the reflection coefficient is measured for the same cell, and in the highest frequency range (500 MHz to 5 GHz), the reflection coefficient is measured by employing a shorter coaxial cell.

Figure 3 shows the measurement system as described in this paper. It consists of two measurement cells, equipment for temperature control, a network analyser system (Hewlett Packard 8753B and 85047A), an impedance analyser (Hewlett Packard LF 4192A) and a personal computer for data acquisition, processing and presentation.

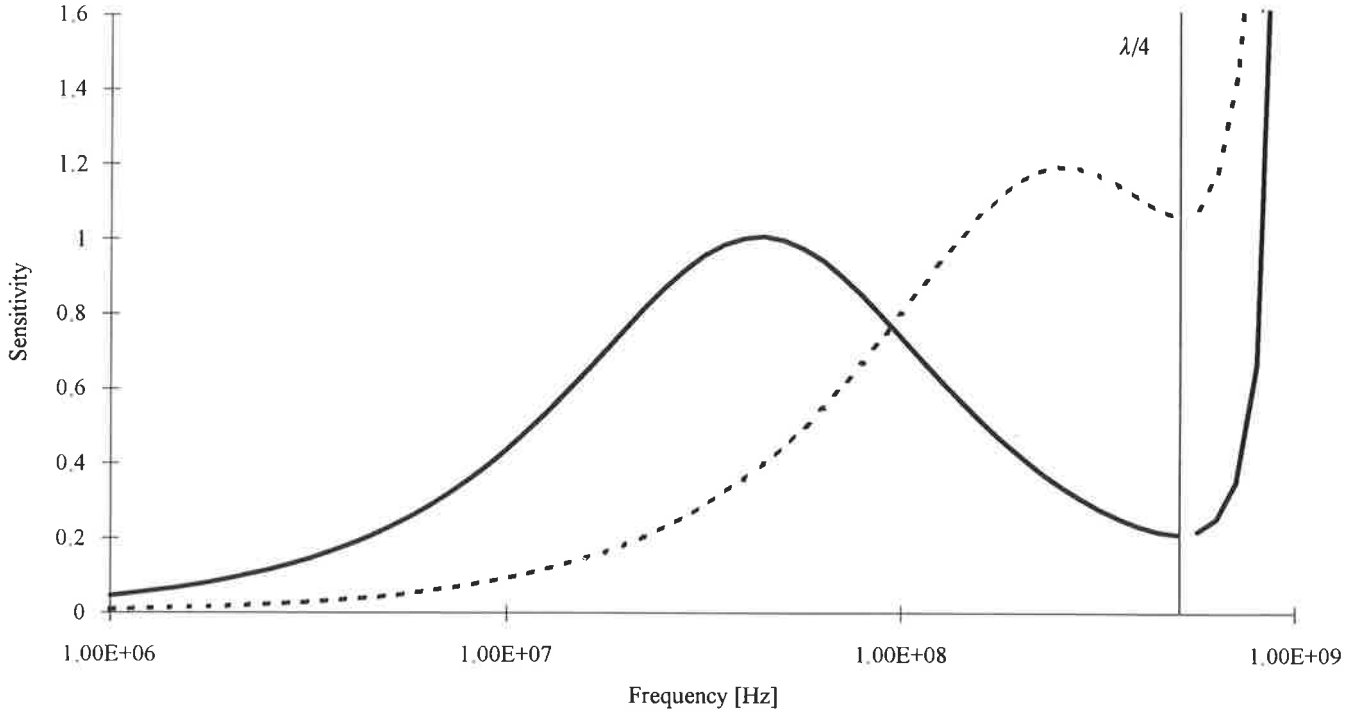

Figure 4. The sensitivity $|(\varepsilon^*/\Gamma)(\partial\Gamma/\partial\varepsilon^*)|$ at $\varepsilon_r^* = 2.2 - j0$ for a cell with $Z_0 = 50\ \Omega$ and $l_e = 10$ cm (– – –) and a cell with $Z_0 = 10\ \Omega$ and $l_e = 10$ cm (——). $\lambda/4$ indicates the position of the quarter-wavelength resonance.

2.1. The design of the impedance cell

In the lowest frequency range, the capacitance and conductance of the low-frequency coaxial measurement cell are measured. The admittance, Y, of the cell filled with a fluid of complex permittivity $\varepsilon_0\varepsilon^* = \varepsilon_0(\varepsilon' - j\varepsilon'')$ is given by

$$\begin{aligned} Y &= j\omega C + G \\ &= j\omega\varepsilon^* C_0 \\ &= j\omega\varepsilon' C_0 + \omega\varepsilon'' C_0 \end{aligned} \tag{2}$$

where C is the capacitance, G the conductance and C_0 the geometric capacitance given by

$$C_0 = \frac{2\pi\varepsilon_0 l_e}{\ln(b/a)} \tag{3}$$

where l_e is the electrical length of the measurement cell, b is the inner radius of the outer conductor and a the radius of the inner conductor. Owing to existing stray capacitances at the end of the cell, the electrical length, l_e, is not equal to the mechanical length, l_m. It is difficult to estimate the electrical length accurately, hence C_0 must be determined numerically. This is explained in section 3.1.

The measurement cell is designed to be sensitive to small changes in the permittivity. This means that the geometric capacitance must be maximized. To minimize the influence of impurities in the measured liquid, a large sample volume is needed. To achieve this, in combination with high geometric capacitance, the cell has to be long. Based on this, a cell with geometric capacitance of approximately 34 pF and mechanical length of 10 cm was designed.

2.2. The design of reflection cells

For frequencies above 10 MHz the reflection coefficient is measured by means of a network analyser system. The complex reflection coefficient is given as [19]

$$\Gamma(\omega) = \frac{Z_C - Z_0}{Z_C + Z_0} \tag{4}$$

where Z_0 is the characteristic impedance of the coaxial line (typically 50 Ω), and Z_C is the impedance of the measurement cell. The impedance of an ideal open-ended cell is [19]

$$Z_C = -j\frac{Z_{C0}}{\sqrt{\varepsilon^*}}\cot\left(\frac{\omega l_e}{c}\sqrt{\varepsilon^*}\right) \tag{5}$$

where Z_{C0} is the characteristic impedance of the cell and c is the velocity of light. Combining equations (4) and (5) relates the permittivity to the measured reflection coefficient.

When designing a measurement cell, there are two parameters that can be varied; the characteristic impedance, Z_{C0}, and the length of the cell, l_e. The length constrains the frequency range of the cell. In this work low-loss liquids with small variations in permittivity are studied. This means that the cell has to be long to introduce the necessary phase shift. However, the maximum length of the cell is restricted by the quarter-wavelength resonance given by

$$l_e < \frac{c}{4f\sqrt{\varepsilon'}}. \tag{6}$$

The characteristic impedance, Z_{C0}, of the cell determines the width of the frequency range to which the cell is

Table 1. Permittivity data including estimated uncertainty for reference fluids at 20 °C found in the literature. Uncertainties in the parameters are estimated by the standard deviation when several independent values are available. When the measurement uncertainty is reported together with the results, this value is used.

Medium	ε_s	ε_∞	τ (ps)	α	Reference
Air	1.0005±0.0002				[22]
Carbon tetrachloride	2.238±0.002				[20]
Chloroform	4.82±0.02	2.28±0.09	6.25±0.1		[23]
Thiophene	2.769±0.002	2.33±0.09	2.7±0.1	0.01±0.01	[20]
Ethyl acetate	6.04±0.02	2.48±0.09	4.4±0.1	0.06±0.01	[20]
Dichloromethane	9.1±0.2				[24]
1,1,1-Trichloroethane	7.2±0.1	2.08±0.02	5.5±0.1	0.030±0.002	[20]
1,2-Dichloroethane	10.65±0.05	2.4±0.1	7.4±3		[20. 24]
Ethyl ether	4.34±0.01	1.85±0.04	2.3±1		[20, 23]
n-Pentane	1.844±0.009				[24]
Monochlorobenzene	5.699±0.008	2.5±0.1	12.5±0.3		[20, 23]
Toluene	2.40±0.02	2.25±0.01	7.34±0.2		[20, 23]
n-Heptane	1.924±0.002				[20, 23, 24]
n-Decane	1.991±0.01				[24]

sensitive. This can be illustrated by keeping the length constant and plotting the sensitivity in the reflection coefficient

$$\left|\frac{\varepsilon^*}{\Gamma}\frac{\partial\Gamma}{\partial\varepsilon^*}\right|$$

in the relevant frequency range for different values of the characteristic impedance (see figure 4). The sensitivity of a 50 Ω cell is highest at frequencies near resonance. By lowering the characteristic impedance, the sensitivity range is moved away from the resonance frequency. This results in a broader frequency range for the cell, as shown in figure 4, but also a smaller sample volume. A compromise is obtained with a characteristic impedance in the range 10–30 Ω [6, 7]. Figure 4 shows that the cell has a limited frequency range depending on the accuracy requirements. A reflection cell typically covers one decade.

Based on equations (4)–(6) and the sensitivity function

$$\left|\frac{\varepsilon^*}{\Gamma}\frac{\partial\Gamma}{\partial\varepsilon^*}\right|$$

the cells for the intermediate- and high-frequency ranges were designed. This gave a mechanical length l_m = 10 cm and a characteristic impedance Z_{C0} = 10 Ω for the intermediate frequency cell. This design was chosen so that the cell could also be used for impedance measurements in the low-frequency range. The cell for the highest frequency range was designed with a 3 mm long centre conductor and characteristic impedance of 20 Ω.

3. Models for determining the permittivity

The models introduced in section 2 are used to achieve optimal cell design. In this section the models relating the measured data to permittivity are presented. As indicated in figure 1, two different models are employed; a linear model for impedance data in the lowest frequency range (< 10 MHz) and a bilinear model for reflection data in the highest frequency range (> 10 MHz).

3.1. The estimated permittivity from the measured impedance

Owing to the fact that it is difficult to develop an exact analytical model for the measurement cell, this system is based upon a numerical calibration of the relationship between measured capacitance, C_{meas} (F), and the real part of the fluid permittivity. The numerical expression is generally presented as

$$C_{meas} = C_P + C_0\varepsilon' \tag{7}$$

The model parameters C_P (F) and C_0 (F) are determined by linear regression on fluids of known permittivity, where C_P represents stray capacitances and C_0 the geometric capacitance of the measurement cell. The fluids employed in the calibration procedure are given in table 1. The measurements were done at 100 kHz. It was found that C_0 = 35.01 pF and C_P = 5.95 pF. This value of C_0 does not differ much from the geometric capacitance of 34 pF for which the cell was designed.

The numerical calibration depends on accurate literature data of both the real and the imaginary parts of the permittivity. The real part of the permittivity is determined from the measured capacitance, C_{meas}, by employing equation (7).

References in the literature on the imaginary part of the permittivity of low-loss fluids involve large uncertainties [20]; hence an accurate linear regression model is difficult to obtain. The estimation of the dielectric loss in this system is therefore based on equation (2):

$$\varepsilon'' = G_{meas}/(\omega C_0) \tag{8}$$

where G_{meas} (S) is the measured conductance containing contributions from both fluid conductivity and dielectric

loss. This modelling procedure is acceptable as long as there is no electrode polarization present. When electrode polarization occurs, a large capacitance will be present in series with the capacitance of the fluid under test [21]. As a consequence, the estimated permittivity at low frequencies will be too high. More work has to be performed in order to model or eliminate the effects of electrode polarization.

3.2. The estimated permittivity from the measured reflection coefficient

Equations (4) and (5) relating reflection coefficient and permittivity are based on ideal conditions, and do not take into account existing stray capacitances, internal reflections, inaccurate mechanical dimensions and so on. The equations are sufficient for theoretical studies and design of measurement cells, but they are not suitable for precise calculation of permittivity. Instead, a model based on Cole's bilinear calibration routine [6] is used. This model includes two calibration fluids and one reference fluid of known permittivity. The permittivity of an unknown sample can be expressed as [7]

$$\varepsilon^* = \frac{A\rho + \varepsilon^*_{\text{ref}}}{1 - B\rho} \tag{9}$$

where

$$\rho = \frac{\Gamma_{\text{ref}} - \Gamma_{\text{x}}}{\Gamma_{\text{ref}} + \Gamma_{\text{x}}} \tag{10}$$

where $\varepsilon^*_{\text{ref}}$ is the relative permittivity of the reference fluid, Γ_{x} is the measured reflection coefficient of the unknown fluid and Γ_{ref} is the measured reflection coefficient of the reference fluid. The complex calibration coefficients A and B represent the measurement cell and connection lines, and take care of all spurious effects. A and B are found by measuring the reflection coefficients of two fluids with known permittivity.

4. Experimental routines and uncertainty estimation

The experimental routines are very important in order to obtain accurate measurements of the impedance and reflection coefficients. Factors like calibration routines, handling of the measurement cells, temperature control and measurement routines have been carefully considered in order to obtain an optimal system. To verify the accuracy in the measurements, the overall uncertainty for the system is estimated.

4.1. Experimental procedures

Measurements on well-defined reference liquids have shown that the experimental procedures have great influence on the accuracy of the system. In the highest frequency range, it is especially important to keep the cables and measurement cells as stable as possible. In this frequency range, a high-quality coaxial cable with a minimized number of connections is used.

Calibration of the analysers with the end of the cables as the calibration plane is followed by measurements on reference and calibration fluids. Between measurements, suitable cleaning fluids are introduced into the cell, which is dried by blowing air through it as indicated in figure 2.

4.2. The estimation of measurement uncertainty

The method of the Bureau International des Poids et Mesures (BIPM) [25] is used to analyse and quantify the measurement uncertainties. All calculations are based on one standard deviation.

When analysing oils, differences in measured permittivity, that is sensitivity, are of more interest than absolute values. If the calibration parameters (the regression line and the parameters in the bilinear calibration formula) are kept constant for different fluids, then the difference can be calculated with improved accuracy compared with the accuracy from differences of independent measurements. In the low-frequency range the difference is found from equations (7) and (8):

$$\varepsilon'_j - \varepsilon'_k = \frac{C_{\text{meas},j} - C_{\text{meas},k}}{C_0} \tag{11}$$

$$\varepsilon''_j - \varepsilon''_k = \frac{C_{\text{meas},j} - C_{\text{meas},k}}{\omega C_0} \tag{12}$$

and in the intermediate- and high-frequency ranges from equation (9):

$$\varepsilon^*_j - \varepsilon^*_k = \frac{A + \varepsilon^*_{\text{ref}} B}{(1 - B\rho_j)(1 - B\rho_k)}(\rho_j - \rho_k) \tag{13}$$

where indices j and k indicate two different fluids.

The main contributions to the uncertainty in the complex permittivity are from the impedance, reflection coefficient and reference parameters (Cole–Cole parameters for the reference fluids). These are the only contributions considered in this work.

Additional contributions to the uncertainty in measured permittivity are impurities in the reference fluids and lack of validity of the models. Electrode polarization in the low-frequency range, cavity resonance and mode conversion in the upper frequency range are not modelled. Electrode polarization is a major source of error when present (it is not present in the measurements presented in this paper). Cavity resonance and mode conversion are assumed to be negligible.

4.2.1. The uncertainty in the model parameters. Uncertainties in the Cole–Cole parameters of the reference fluids in table 1 are estimated by the standard deviation when several independent values are available. When the measurement uncertainty is reported together with the results, this value is used. Uncertainty in the temperature due to the control and heat loss is estimated to be 0.5 °C, which has a negligible effect on the complex permittivity.

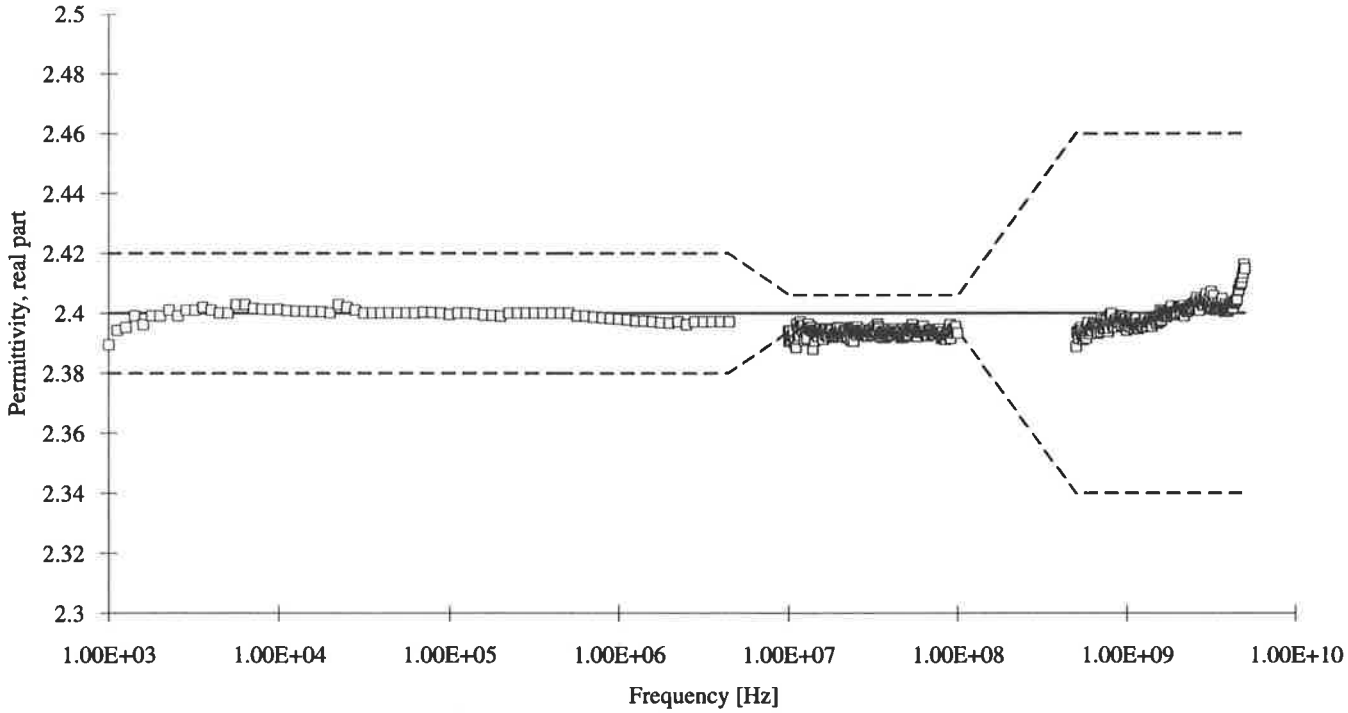

Figure 5. The real part of the dielectric spectrum of toluene from 1 kHz to 5 GHz: (□), the measured permittivity; (——), the literature value; and (– – –), the overall uncertainty limit. Compared with literature data ($\varepsilon' = 2.40 \pm 0.02$), the system determines the permittivity within two combined uncertainties as estimated in table 2.

Calculation of C_p and C_0 by linear regression is described in section 3.1. Uncertainties are calculated from the regression statistics and estimated to be

$$\Delta C_0 = 0.082 \text{ pF} \tag{14}$$

$$\Delta C_P = 0.35 \text{ pF} \tag{15}$$

To estimate the uncertainty in the measured impedance and reflection coefficient, and to examine the repeatability of the filling and cleaning process, measurements were performed when the cells were filled with toluene. The measurements were repeated 17 times. Between each filling, the cells were cleaned and dried, and approximately 10 min temperature stabilization time was used before each measurement. The total time of the experiment was about 3.5 h. During the experiment, the ambient temperature was stable at 20 °C.

Owing to the calibration procedure systematic errors in the measured capacitance are compensated for, assuming that these errors are frequency-independent. The uncertainty in capacitance, ΔC_{meas}, is therefore estimated from the standard deviation of the repeated measurements of C:

$$\Delta C_{meas} = 0.06 \text{ pF}. \tag{16}$$

Systematic, as well as random, errors in the measured conductance contribute to the uncertainty in the imaginary part of the permittivity in the lowest frequency range. ΔG_{meas} is therefore obtained by combining the average and standard deviation of the repeated measurements of G:

$$\Delta G_{meas} = 0.8 f \text{ pS}. \tag{17}$$

Systematic errors in the reflection coefficient are also compensated for. In the highest frequency ranges, the uncertainties in the amplitude and phase of the measured reflection coefficient are estimated by the standard deviation of the repeated measurements. Uncertainties in the real and imaginary parts are calculated from these and are given in equations (18) and (19):

$$\Delta\Gamma_{Re} = \begin{cases} 0.0005 & 10 \text{ MHz} \leqslant f \leqslant 100 \text{ MHz} \\ 0.01[(0.1\cos\phi)^2 + (\sin\phi)^2]^{1/2} & \\ & 0.5 \text{ GHz} \leqslant f \leqslant 5 \text{ GHz} \end{cases} \tag{18}$$

$$\Delta\Gamma_{Im} = \begin{cases} 0.0005 & 10 \text{ MHz} \leqslant f \leqslant 100 \text{ MHz} \\ 0.01[(0.1\sin\phi)^2 + (\cos\phi)^2]^{1/2} & \\ & 0.5 \text{ GHz} \leqslant f \leqslant 5 \text{ GHz} \end{cases} \tag{19}$$

where ϕ is the phase of the measured reflection coefficient.

4.2.2. The combined uncertainty in permittivity. The uncertainty in the measured relative complex permittivity is calculated by combining the different contributions. In the low-frequency range the only significant contributions to the uncertainty in the real part of the permittivity, $\Delta\varepsilon'$, are the uncertainties in C_P and C_0, ΔC_P and ΔC_0 respectively. The only significant contribution to the uncertainty in the imaginary part of the permittivity, $\Delta\varepsilon''$, is ΔG_{meas}. This gives

$$(\Delta\varepsilon')^2 \approx \left(\frac{\Delta C_P}{C_0}\right)^2 + \left(\frac{C_{meas} - C_P}{C_0^2}\Delta C_0\right)^2 \tag{20}$$

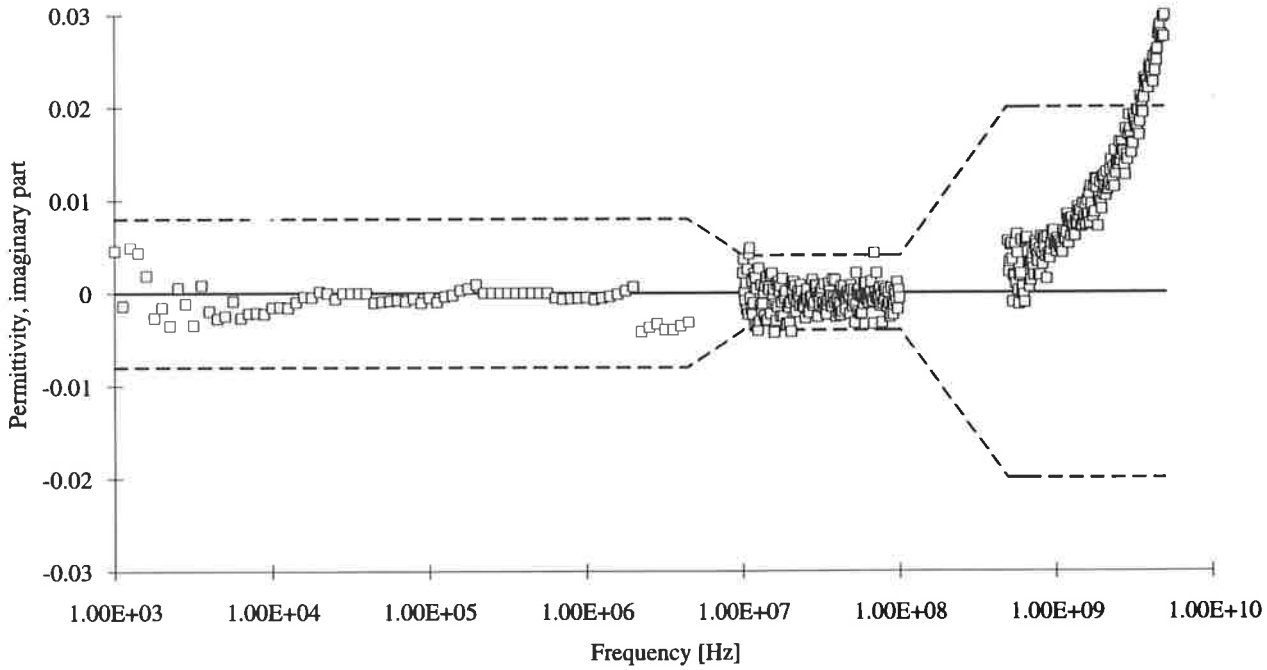

Figure 6. The imaginary part of the dielectric spectrum of toluene from 1 kHz to 5 GHz: (□), the measured permittivity; (——), the literature value; and (– – –), the overall uncertainty limit. Compared with literature data ($\varepsilon'' = 0$), the system determines the permittivity within two combined uncertainties as estimated in table 2 for most of the frequencies.

Table 2. The calculated uncertainty in the measured absolute permittivity for toluene.

Frequency range	$\Delta\varepsilon'_{tol}$	$\Delta\varepsilon''_{tol}$
1 kHz to 5 MHz	0.01	0.004
10–100 MHz	0.003	0.002
0.5–5 GHz	0.03	0.01

Table 3. The calculated uncertainty in the measured difference in permittivity between toluene and n-pentane.

Frequency range	$\Delta(\varepsilon'_{tol} - \varepsilon'_{pen})$	$\Delta(\varepsilon''_{tol} - \varepsilon''_{pen})$
1 kHz to 5 MHz	0.002	0.005
10–100 MHz	0.002	0.002
0.5–5 GHz	0.03	0.01

$$(\Delta\varepsilon'')^2 \approx \left(\frac{\Delta G_{meas}}{\omega C_0}\right)^2. \tag{21}$$

In the intermediate- and high-frequency ranges the partial derivative in equations (22), (23), (26) and (27) are dependent on the values of the permittivities of the calibration and reference fluids. Best results are obtained when the reference fluid has permittivity close to the unknown fluid, and when the calibration fluids span the permittivity range of interest. The main contributions to the uncertainty in the permittivity are the uncertainties in the measured reflection coefficients for the unknown and the reference fluids, and the uncertainty in the permittivity of the reference fluid. This gives

$$(\Delta\varepsilon')^2 \approx \left[\mathrm{Re}\left(\frac{\partial\varepsilon^*}{\partial\varepsilon^*_{ref}}\right)\Delta\varepsilon'_{ref}\right]^2 + \left[\mathrm{Im}\left(\frac{\partial\varepsilon^*}{\partial\varepsilon^*_{ref}}\right)\Delta\varepsilon''_{ref}\right]^2 + \left[\mathrm{Re}\left(\frac{\partial\varepsilon^*}{\partial\Gamma_{ref}}\right)\Delta\Gamma_{Re,ref}\right]^2 + \left[\mathrm{Im}\left(\frac{\partial\varepsilon^*}{\partial\Gamma_{ref}}\right)\Delta\Gamma_{Im,ref}\right]^2 + \left[\mathrm{Re}\left(\frac{\partial\varepsilon^*}{\partial\Gamma_x}\right)\Delta\Gamma_{Re,x}\right]^2 + \left[\mathrm{Im}\left(\frac{\partial\varepsilon^*}{\partial\Gamma_x}\right)\Delta\Gamma_{Im,x}\right]^2 \tag{22}$$

$$(\Delta\varepsilon'')^2 \approx \left[\mathrm{Im}\left(\frac{\partial\varepsilon^*}{\partial\varepsilon^*_{ref}}\right)\Delta\varepsilon'_{ref}\right]^2 + \left[\mathrm{Re}\left(\frac{\partial\varepsilon^*}{\partial\varepsilon^*_{ref}}\right)\Delta\varepsilon''_{ref}\right]^2 + \left[\mathrm{Im}\left(\frac{\partial\varepsilon^*}{\partial\Gamma_{ref}}\right)\Delta\Gamma_{Re,ref}\right]^2 + \left[\mathrm{Re}\left(\frac{\partial\varepsilon^*}{\partial\Gamma_{ref}}\right)\Delta\Gamma_{Im,ref}\right]^2 + \left[\mathrm{Im}\left(\frac{\partial\varepsilon^*}{\partial\Gamma_x}\right)\Delta\Gamma_{Re,x}\right]^2 + \left[\mathrm{Re}\left(\frac{\partial\varepsilon^*}{\partial\Gamma_x}\right)\Delta\Gamma_{Im,x}\right]^2 \tag{23}$$

where ε^* is given by equation (9). This uncertainty is somewhat frequency-dependent and is minimum in the middle of the frequency range of the cells.

For differences in permittivity, the uncertainty is mainly dependent on the uncertainty in the measured parameters for the fluids under test. Contributions from calibration and reference fluids are negligible when fluids

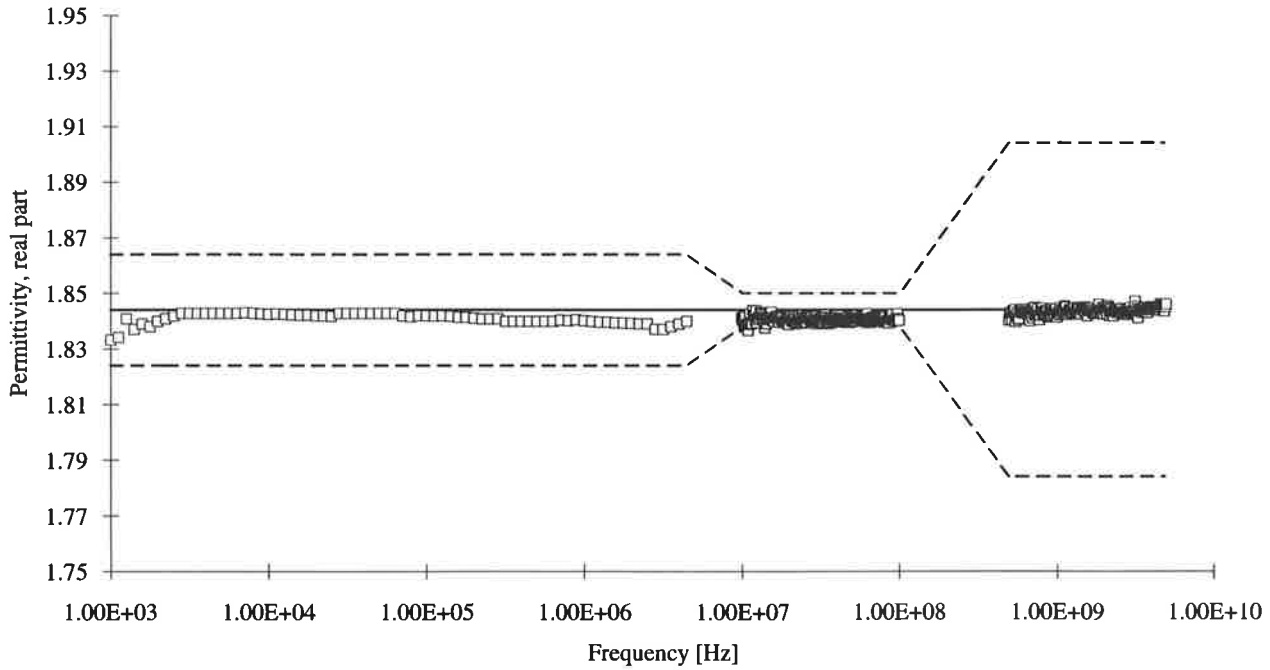

Figure 7. The real part of the dielectric spectrum of n-pentane from 1 kHz to 5 GHz: (□), the measured permittivity; (——), the literature value; and (– – –), the overall uncertainty limit. Compared with literature data ($\varepsilon' = 1.884 \pm 0.009$), the system determines the permittivity within two combined uncertainties as estimated in table 2.

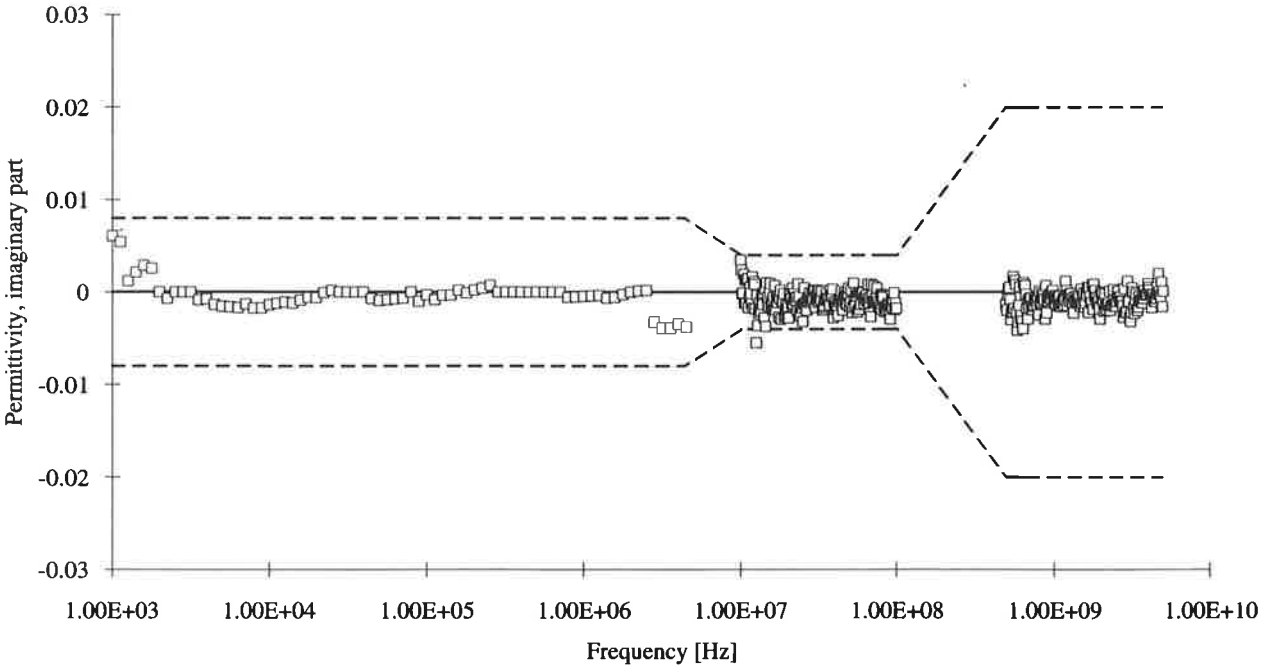

Figure 8. The imaginary part of the dielectric spectrum of n-pentane from 1 kHz to 5 GHz: (□), the measured permittivity; (——), the literature value; and (– – –), the overall uncertainty limit. Compared with literature data ($\varepsilon'' = 0$), the system determines the permittivity within two combined uncertainties as estimated in table 2.

with low uncertainty in the reference parameters (as in table 1) are used, and when the temperature is stable. When the difference in permittivity between two fluids is small, the uncertainty in the low-frequency range is given by

$$\Delta(\varepsilon_j' - \varepsilon_k')^2 \approx 2\left(\frac{\Delta C_{\text{meas}}}{C_0}\right)^2 \tag{24}$$

$$\Delta(\varepsilon_j'' - \varepsilon_k'')^2 \approx 2\left(\frac{\Delta G_{\text{meas}}}{\omega C_0}\right)^2. \tag{25}$$

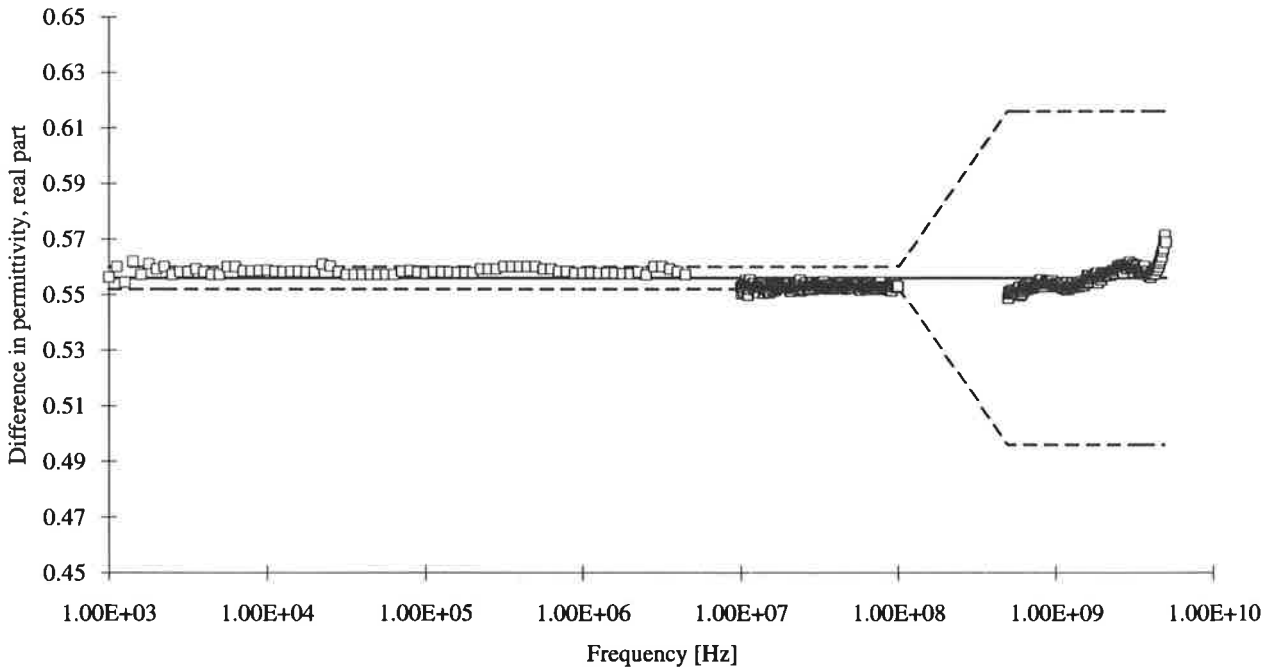

Figure 9. The difference in the real part of the permittivity between toluene and n-pentane: (□), the difference in measured permittivity; (——), the difference in literature values; and (– – –), the overall uncertainty limit. Compared with literature data ($\varepsilon''_{\text{tol}} - \varepsilon''_{\text{pen}} = 0.556$), the system determines the permittivity within two combined uncertainties as estimated in table 3.

This is an improvement in the real part due to the reduced contributions from the regression formula, but the result is the same as for independent measurements for the imaginary part. In the intermediate- and high-frequency ranges, the uncertainties are approximately

$$\begin{aligned}\Delta(\varepsilon'_j - \varepsilon'_k)^2 \approx{}& \left[\mathrm{Re}\left(\frac{\partial(\varepsilon_j^* - \varepsilon_k^*)}{\partial\Gamma_j}\right)\Delta\Gamma_{\mathrm{Re},j}\right]^2 \\ &+ \left[\mathrm{Im}\left(\frac{\partial(\varepsilon_j^* - \varepsilon_k^*)}{\partial\Gamma_j}\right)\Delta\Gamma_{\mathrm{Im},j}\right]^2 \\ &+ \left[\mathrm{Re}\left(\frac{\partial(\varepsilon_j^* - \varepsilon_k^*)}{\partial\Gamma_k}\right)\Delta\Gamma_{\mathrm{Re},k}\right]^2 \\ &+ \left[\mathrm{Im}\left(\frac{\partial(\varepsilon_j^* - \varepsilon_k^*)}{\partial\Gamma_k}\right)\Delta\Gamma_{\mathrm{Im},k}\right]^2 \end{aligned} \tag{26}$$

$$\begin{aligned}\Delta(\varepsilon''_j - \varepsilon''_k)^2 \approx{}& \left[\mathrm{Im}\left(\frac{\partial(\varepsilon_j^* - \varepsilon_k^*)}{\partial\Gamma_j}\right)\Delta\Gamma_{\mathrm{Re},j}\right]^2 \\ &+ \left[\mathrm{Re}\left(\frac{\partial(\varepsilon_j^* - \varepsilon_k^*)}{\partial\Gamma_j}\right)\Delta\Gamma_{\mathrm{Im},j}\right]^2 \\ &+ \left[\mathrm{Im}\left(\frac{\partial(\varepsilon_j^* - \varepsilon_k^*)}{\partial\Gamma_k}\right)\Delta\Gamma_{\mathrm{Re},k}\right]^2 \\ &+ \left[\mathrm{Re}\left(\frac{\partial(\varepsilon_j^* - \varepsilon_k^*)}{\partial\Gamma_k}\right)\Delta\Gamma_{\mathrm{Im},k}\right]^2 . \end{aligned} \tag{27}$$

From equations (20)–(27) it can be seen that the uncertainty in measured complex permittivity can be further reduced by reducing the uncertainty in measured impedance and reflection coefficient.

4.2.3. Numerical calculation of the uncertainty. The uncertainty in permittivity is calculated for toluene and the results are given in table 2. In the intermediate- and high-frequency ranges, air and monochlorobenzene are used as calibration fluids and n-heptane as reference fluid. The uncertainties are in agreement with the calculation of the standard deviation of the permittivity of the repeated measurements. This indicates that all major contributions are incorporated and correctly estimated in the calculations.

The results in table 2 are found to be less (in terms of percentage for $\Delta\varepsilon'_{\text{tol}}$ and absolute value for $\Delta\varepsilon''_{\text{tol}}$) than the uncertainties obtained with the systems in [12, 26–31], but somewhat larger than those for the transmission and discontinuous inner conductor systems in [10] and for the systems in [32, 33]. However, none of the reported uncertainties are for fluids of low permittivity.

The uncertainties are calculated for the difference in permittivity between toluene and n-pentane. The results are given in table 3. Compared with differences of independent measurements, this is an improvement. If the measurements were independent the uncertainties in table 3 would have been $\sqrt{2}$ times the results in table 2.

5. Results

In the evaluation of the developed system and for verification of the uncertainty estimations, measurements were performed on fluids of known permittivity. The overall uncertainty is defined as two combined uncertainties as calculated in section 4.

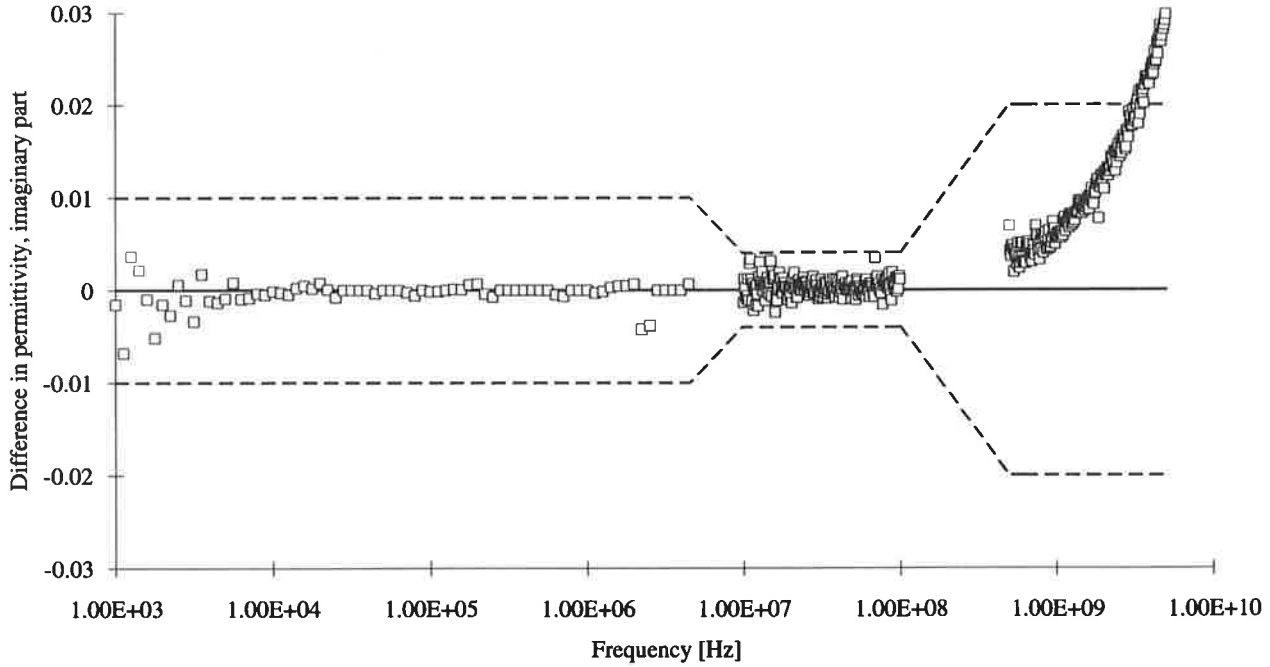

Figure 10. The difference in the imaginary part of the permittivity between toluene and n-pentane: (□), the difference in measured permittivity; (——), the difference in literature values; and (– – –), the overall uncertainty limit. Compared with literature data ($\varepsilon''_{tol} - \varepsilon''_{pen} = 0$), the system determines the permittivity within two combined uncertainties as estimated in table 3.

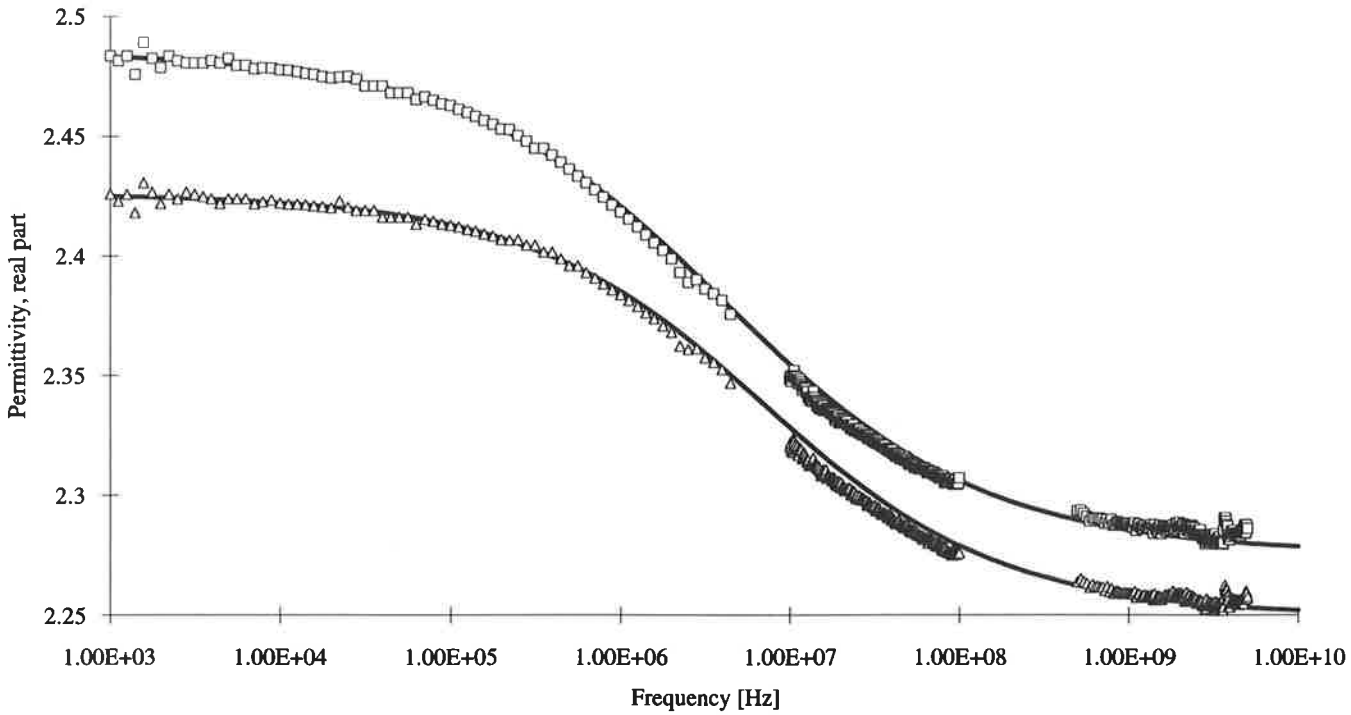

Figure 11. The real part of the measured dielectric spectra of distillation residuals (+300 °C) of Gullfaks field crude oil (□) and of Statfjord crude oil (△). The lines represent the Cole–Cole fitting of the measured spectra.

Figure 5 shows the real part of the measured dielectric spectrum of toluene. The literature value of 2.40 with its estimated overall uncertainty is also shown. From figure 5 it is seen that the calculated permittivity falls within the estimated uncertainty ranges for the lowest and highest frequency ranges. In the intermediate frequency range the uncertainty seems to be somewhat underestimated. However, the deviation from the literature value is less than the uncertainty in it (±0.02, see table 1).

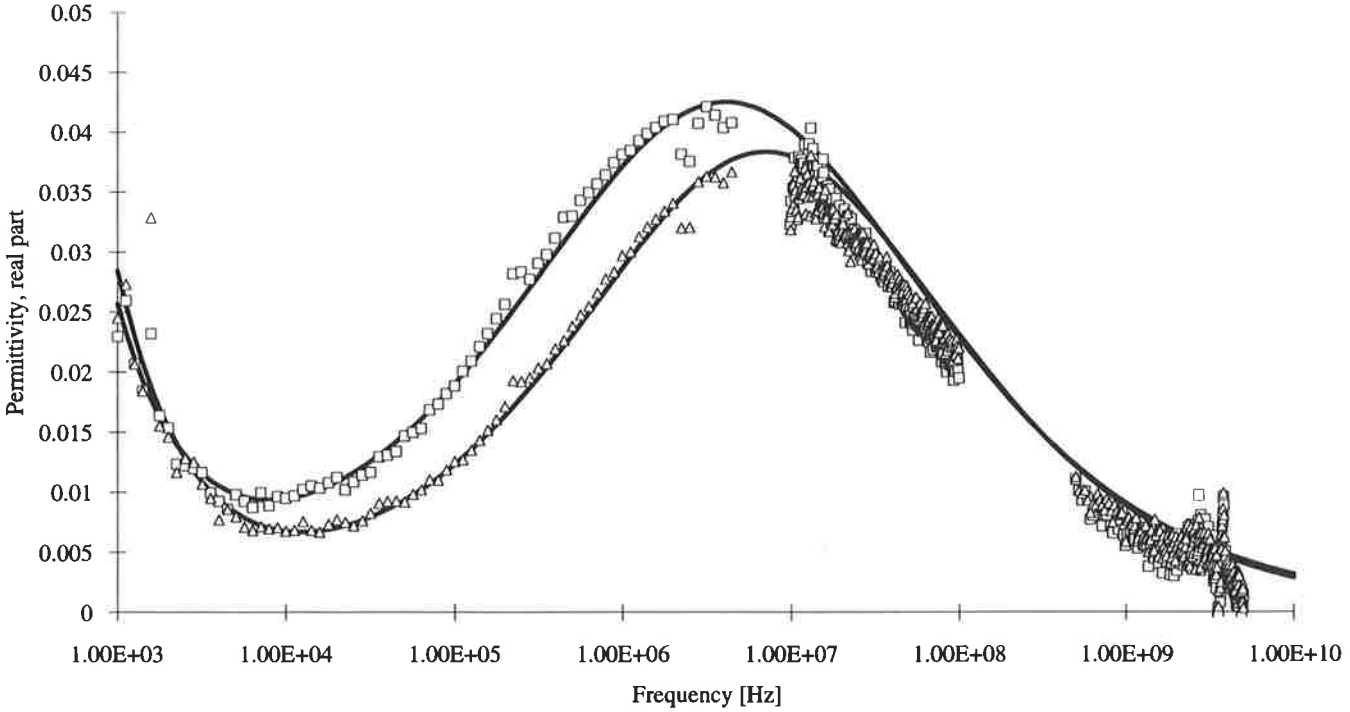

Figure 12. The imaginary part of the measured dielectric spectra of distillation residuals (+300 °C) of Gullfaks field crude oil (□) and of Statfjord crude oil (□). The lines represent the Cole–Cole fitting of the measured spectra.

Figure 6 shows the imaginary part of the dielectric spectrum of toluene together with the literature value and overall uncertainty. The calculated permittivity falls outside the uncertainty range for frequencies above 3 GHz. This may be due to the quarter-wavelength resonance effect, which is not incorporated properly in the uncertainty analysis.

Figures 7 and 8 show the real and imaginary parts of the permittivity for n-pentane together with the literature values and the overall uncertainty. The combined uncertainty for n-pentane is assumed to be the same as for toluene (see table 2). The calculated permittivity is within the overall uncertainty. No resonance effects are seen here, due to the lower permittivity of n-pentane.

Figure 9 shows the measured difference in the real part of the permittivity for toluene and n-pentane when the calibration parameters are the same for both fluids. The calculations in section 4 (see table 3) predict that the uncertainty in these values should be less than the uncertainty in the differences of independent measurements. It is seen that the difference is within the calculated overall uncertainty of the difference in the literature values (which is found to be 0.556). The imaginary part of the permittivity is also within the overall uncertainty (see figure 10), but the overall uncertainty for the imaginary part is about the same size as the uncertainties in the individual measurements as described in section 4.

The measurements on fluids with known permittivity confirm that all major contributions are incorporated in the estimated uncertainty of the system. The next step is to confirm that petroleum products of different qualities have differences in their permittivity spectra that can be detected by the measurement system described in this work. Figures 11 and 12 show the dielectric spectra of two distillation residuals (+300 °C) of North Sea crude oils from the Statfjord and the Gullfaks field. The spectra are fitted to the Cole–Cole model by employing the Levenberg–Marquardt iterative routine [34]. The calculated Cole–Cole parameters are given in table 4. Figures 11 and 12 show that the oils have a low-loss, broad-frequency dispersion region, and that the differences in permittivity between the oils are small. However, the differences are significant, and this is confirmed by the fact that the differences are larger than the overall uncertainty of the measurement system. Figures 11 and 12 confirm that a dielectric measurement system for quality determination of heavy oil must have high sensitivity and a broad frequency range.

Table 4. The calculated Cole–Cole parameters of two distillation residuals (+300 °C) of North Sea crude oils from the Statfjord and the Gullfaks field.

	ε_s	ε_∞	τ (ns)	α	σ (nS m^{-1})
Statfjord residual	2.426	2.249	22.3	0.48	1.5
Gullfaks residual	2.486	2.275	38.4	0.51	1.3

6. Conclusions

A thorough description of a sensitive permittivity measurement system for low-loss, low-permittivity liquids over a broad frequency range has been given.

The sensitivity, accuracy and repeatability of the system has been obtained through a combination of optimal cell design, careful mechanical construction and experimental procedures. Owing to the combination of impedance and reflection measurements, and the use of precise models for permittivity calculation, the system can accurately determine the permittivity over the broad frequency range from 1 kHz to 5 GHz.

The high sensitivity and accuracy of the system is verified through a thorough uncertainty analysis and measurements on fluids with known permittivity. By using the same calibration measurements for calculating the permittivity of different fluids, improved accuracy in permittivity differences is obtained compared with independent measurements. It is found that the overall uncertainty (given as two combined uncertainties) in ε' for low-permittivity fluids is less than 0.8% for frequencies below 100 MHz and within 2.6% for frequencies in the range 0.5–5 GHz. The uncertainty in ε'' is found to be within 0.02 (absolute) in the whole frequency range.

Owing to the high sensitivity of the system it can be used to measure the dielectric spectra of heavy oils. The dielectric loss of heavy oil is very small, there is a large dispersion frequency distribution, and the difference between static and optic permittivity is rather modest. However, the differences between oils of different quality are significant, and it is possible to relate the dielectric spectra to certain bulk quality parameters in the oil [35]. This will be further studied in future work. Refinements of the measurement system and development of an on-line analyser will also be investigated.

Acknowledgments

This work is performed at Christian Michelsen Research AS within the Strategic Technology Programme for On-line Monitoring of Oil and Gas Processes (TOP) supported by the Norwegian Research Council (NRC), Statoil and Norsk Hydro.

References

[1] Tinham B 1994 Putting modern analysers on-line *Control Instrum.* March 37

[2] Clevett K 1994 Process analysers—industry perspectives *C&I* March 29–31

[3] Kemp W 1978 *Organic Spectroscopy* (London: Macmillan)

[4] van der Maas J H 1969 *Basic Infrared Spectroscopy* (London: Heyden)

[5] Smyth C P 1955 *Dielectric Behavior and Structure* (New York: McGraw-Hill)

[6] Cole R H 1983 Bridge sampling methods for admittance measurements from 500 kHz to 5 GHz *IEEE Trans. Instrum. Meas.* **32** 42–7

[7] Cole R H, Berberian J G, Mashimo S, Chryssikos G, Burns A and Tombari E 1989 Time domain reflection methods for dielectric measurements to 10 GHz *J. Appl. Phys.* **66** 793–802

[8] Cole K S and Cole R H 1941 Dispersion and absorption in dielectrics I. Alternating current characteristics *J. Chem. Phys.* **9** 341–51

[9] Debye P 1929 *Polar Molecules* (New York: Chemical Catalogue Company)

[10] Jenkins S, Hodgetts T E, Clarke R N and Preece A W 1990 Dielectric measurements on reference liquids using automatic network analysers and calculable geometries *Meas. Sci. Technol.* **1** 691–702

[11] Cole R H, Mashimo S and Winsor IV P 1980 Evaluation of dielectric behavior by time domain spectroscopy. 3. Precision difference methods *J. Phys. Chem.* **84** 786–93

[12] Hill G J 1993 Traceable dielectric measurements by resonance methods in the frequency range 1–30 MHz *Proc. IEE* **140** 382–4

[13] von Hippel A 1954 *Dielectrics and Waves* (New York: Wiley)

[14] von Hippel A 1954 *Dielectric Materials and Applications* (New York: Wiley)

[15] Sakamoto T, Nakamura H, Uedaira H and Wada A 1989 High-frequency dielectric relaxation of water bound to hydrophilic silica gels *J. Phys. Chem.* **93** 357–66

[16] Gestblom B and Sjøblom J 1984 Dielectric relaxation studies of aqueous long-chain alcohol solutions *Acta Chem. Scand.* A **38** 47–56

[17] Gestblom B and Elmgren H 1982 A transmission dielectric time domain spectroscopy method for aqueous systems *Chem. Phys. Lett.* **90** 412–16

[18] Somlo P I 1993 A convenient self-checking method for the automated microwave measurement of μ and ε *IEEE Trans. Instrum. Meas.* **42** 213–16

[19] Ramo S, Whinnery J R and van Duzer T 1965 *Fields and Waves in Communication Electronics* (New York: Wiley)

[20] Buckley F and Maryott A A 1958 *Tables of Dielectric Dispersion Data for Pure Liquids and Dilute Solutions* (New York: National Bureau of Standards)

[21] Schwan H P 1963 Physical techniques in biological research *Determination of Biological Impedances* ed G Oster (New York: Academic)

[22] Weast R C and Astle M J 1981 *Handbook of Chemistry and Physics* (Boca Raton, FL: CRC)

[23] Akhadov Y Y 1980 *Dielectric Properties of Binary Solutions* (Oxford: Pergamon)

[24] Maryott A A and Smith E R 1951 *Table of Dielectric Constants of Pure Liquids* (New York: National Bureau of Standards)

[25] Giacomo P 1981 News from BIPM *Metrologia* **17** 69–74

[26] Otto G P and Chew W C 1991 Improved calibration of a large open-ended coaxial probe for dielectric measurements *IEEE Trans. Instrum. Meas.* **40** 742–6

[27] Mashimo S, Umehara T, Ota T, Kuwabara S, Shinyashiki N and Yagihara S 1987 Evaluation of complex permittivity of aqueous solution by the time domain reflectometry *J. Mol. Liquids* **36** 135–51

[28] Nyshadham A, Sibbald C L and Stuchly S S 1992 Permittivity measurements using open-ended sensors and reference liquid calibration—an uncertainty analysis *IEEE Trans. Microwave Theory Tech.* **40** 305–14

[29] Jiang G Q, Wong W H, Raskovich E Y, Clark W G, Hines W A and Sanny J 1993 Open-ended coaxial-line technique for measurement of the microwave dielectric constant for low-loss solids and liquids *Rev. Sci. Instrum.* **64** 1614–26

[30] Burdette E C, Cain F L and Seals J 1980 *In vivo* probe measurement technique for determining dielectric properties at VHF through microwave frequencies *IEEE Trans. Microwave Theory Tech.* **28** 414–27

[31] Marsland T P and Evans S 1987 Dielectric measurements with an open-ended coaxial probe *Proc. IEE* **134** 341–9

[32] Athey T W, Stuchly M A and Stuchly S S 1982 Measurement of radio frequency permittivity of biological tissues with an open-ended coaxial line: part I *IEEE Trans. Microwave Theory Tech.* **30** 82–6

[33] Gabriel C, Sheppard R J and Grant E H 1983 Dielectric properties of ocular tissues at 37 °C *Phys. Med. Biol.* **28** 43–9

[34] Press W H, Teukolsky S A, Vetterling W T and Flannery B P 1992 *Numerical Recipes in C. The Art of Scientific Computing* (New York: Cambridge University Press)

[35] Tjomsland T, Hilland J, Christy A A, Sjøblom J, Riis M, Friisø T and Folgerø K Comparison of infrared and impedance spectra of petroleum fractions *Fuel* submitted